II. RADIO ASTRONOMY*

Academic and Research Staff

Prof. A. H. Barrett
Prof. B. F. Burke
Prof. R. M. Price
Prof. D. H. Staelin
Dr. G. D. Papadopoulos
J. W. Barrett
D. C. Papa

Graduate Students

R. H. Cohen
P. C. Crane
M. S. Ewing
T. D. Halket
H. F. Hinteregger
P. L. Kebabian
C. A. Knight
K-S. Lam
K-Y. Lo
P. C. Myers
R. K. L. Poon
P. W. Rosenkranz
P. R. Schwartz
J. H. Spencer
J. W. Waters
A. R. Whitney

A. FORMALDEHYDE ABSORPTION IN THREE DARK GALACTIC CLOUDS

1. Introduction

A study of formaldehyde absorption at 4.83 GHz in three dark galactic clouds was made in April 1971 with the 140 ft telescope of the National Radio Astronomy Observatory in Green Bank, West Virginia. Each cloud was mapped extensively in order to gain information about its formaldehyde distribution, its spatial structure, its group and internal motions. This report discusses the observations and initial findings.

2. Equipment and Observing Procedure

The 140 ft telescope was equipped with a cooled 6-cm parametric amplifier and a 413-channel autocorrelator. Spectral resolutions of 3.25 and 6.50 kHz were used. The system temperature ranged from 78°K to 95°K, with 85°K a typical value. The radiometer employed frequency switching in the first local oscillator at a rate of 1 Hz. Scans across Virgo A produced a peak continuum temperature of 17.9°K and half-power beamwidths of 7.1' and 6.8' in Right Ascension and Declination, respectively. A mean aperture efficiency of 0.47 was computed by adopting values of 78 flux units for Virgo A and 20 flux units for DR 21.

For each cloud, data were taken over a grid of positions, with a typical line detection lower limit of 0.1 K. A coarse grid of positions separated by several beamwidths was made first; regions that yielded interesting spectra were then studied more carefully by filling in the grid. The frequency switching scheme overlapped signal and comparison bands by half a bandwidth, so that post real-time processing would yield

*This work was supported principally by the National Aeronautics and Space Administration (Grants NGL 22-009-016 and NGL 22-009-421), and the National Science Foundation (Grant GP-20769); and in part by California Institute of Technology Contract 952568, and the Sloan Fund for Basic Research (M.I.T. Grant 241).

higher sensitivity in the radial velocity range where detection was expected. Two sample spectra are shown in Fig. II-1.

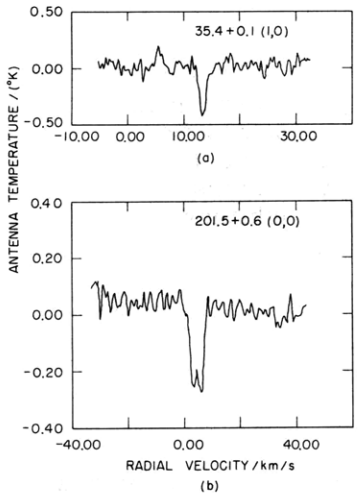

Fig. II-1. Spectra from 35.4+0.1 and 201.5+0.6 in the velocity ranges where signal and comparison bands overlap. The ordered pair is the offset from the reference position in Right Ascension, and in Declination, in units of 6 minutes of arc. In (a), the apparent emission feature at 6 km/s is actually an absorption line at +44 km/s.

3. Results of Observations.

The observational results are summarized in Table II-1. The velocity range listed is the total range spanned by the signal and comparison bands. In cloud 35.4+0.1, the two highest velocity features were detected because they fell in the comparison band and appeared in the difference spectra as emission lines. Later observations with a

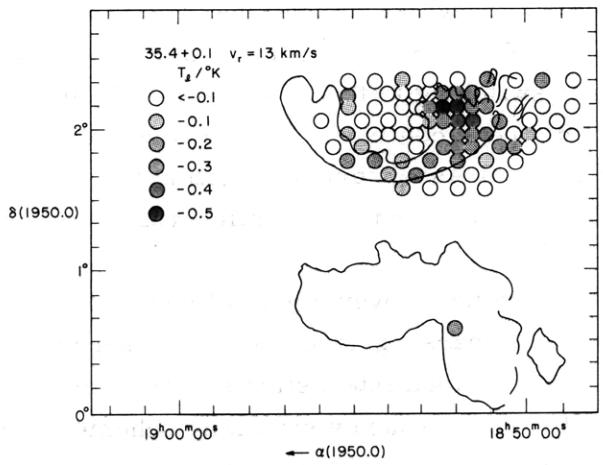

Fig. II-2. Absorption line intensity distribution for 35.4+0.1, radial velocity = 13 km/s. Circles represent half-power beam shapes located at the angular positions where data were taken. The radio diagram is superimposed on a tracing of a Palomar Sky Atlas photograph of the cloud.

Table II-1. Summary of observations.

Source	Reference Position (1950) α(h, m, s)	δ(°, ', ")	Velocity Range (km/s)	Frequency Resolution (kHz)	Positions Observed	Detection Velocities (km/s)	No. of Detections	Line Temperatures (K)
35.4 + 0.1	18 53 07	02 09 49	-45 to 71	3.25	78	9	4	-.1 to -.3
						13	38	-.1 to -.5
						29	3	-.1 to -.2
						44	13	-.1 to -.3
						53	4	-.1 to -.3
127.7 + 14.0	02 04 31	75 55 07	-55 to 61	3.25	56	-38	4	-.1 to -.2
						3	14	-.1 to -.3
						8	3	-.1 to -.2
						18	4	-.1 to -.2
						19	3	-.1 to -.2
201.5 + 0.6	06 29 52	10 32 22	-112 to 120	6.50	62	4	23	-.1 to -.3

higher velocity signal band showed them to be absorption lines. A velocity of formaldehyde detection is listed only if the feature was detected in three or more positions.

The angular distribution of detected formaldehyde varies considerably from one cloud to the next. In 35.4+0.1, small clumps of formaldehyde appear off the southwest, north, and west edges of the optical cloud image at 9, 29, and 53 km/s, respectively. Formaldehyde moving along the line of sight at 13 km/s coincides largely with the optical image; it is the strongest and most widespread feature observed. The distribution of absorption line intensity for this feature is presented in Fig. II-2. At 44 km/s, a ring of detections appears, with a diameter approximately half the east-west diameter of the optical image. The strongest detections appear off the edge of both the optical image and the 13 km/s radio image.

In cloud 127.7+14.0, formaldehyde detected at each velocity appears in clumps in either the eastern or western parts of the cloud, or in both. The central region appears devoid of formaldehyde, except for a few features, each present in only one angular position. In 201.5+0.6, formaldehyde is present only at 4 km/s, and only in a sharply-defined region in the south central part of the optical image.

4. Discussion of the Results.

The location of 35.4+0.1 along a direction in the galaxy with much neutral hydrogen and dust suggests that the several detection velocities may correspond to several clouds or clumps of gas, spatially separated along the line of sight. Only one radio image, at 13 km/s, corresponds to the optical image; the others may be closer to earth, or farther away. The velocity distribution of formaldehyde in 127.7+14.0 is not as easy to explain. The line of sight to this cloud is at a galactic longitude where little neutral hydrogen is found. Furthermore, the high galactic latitude of $b^{II} = 14.0$ means that the line of sight is within the galactic disk for only approximately 900 parsecs, under the assumption of a disk thickness of 210 parsecs. This distance is less than 0.1 of the in-the-plane line-of-sight length for the other two clouds observed. The amount of intercepted material should therefore be much lower. If the galactic formaldehyde distribution follows that of neutral hydrogen and dust, then fewer separate formaldehyde clouds should be seen. In the case of 201.5+0.6, the single detection velocity is consistent with the low concentration of dust and neutral hydrogen along the line of sight.

A detailed analysis of these observations, as well as observations of the same clouds at the 1.667 GHz transition of the OH radical, will be published later.

P. C. Myers, A. H. Barrett

B. STELLAR INTERFEROMETER

During this quarter the duplicating filters described in our last report[1] have been constructed, and operate as expected. Each unit cell occupies a 2.5 in. × 4.5 in. double-sided etched board. Although the dual 100-bit MOS shift registers that are used are designed for DTL or TTL voltage levels, the availability of RTL gates with a minimum open-circuit output voltage of 2.6 V makes it possible for them to be used with RTL. The shift registers are used with a substrate voltage of +5 V, and a clamping diode has been provided to prevent the substrate from being forward-biased if the 5 V supply should fail while the 3.6 V supply for the RTL is on. The lot of 35 shift registers obtained for this project was tested initially to see if they could be used with the substrate at +3.6 V. Since the shift registers are P channel MOS, the limiting factor in this case is that when the bipolar logic is in the low state, the voltage must be far enough below the substrate that a channel is formed in the input transistor of the shift register. In half of the units tested, the threshold was low enough that operation at this substrate voltage would be possible. Therefore a design with the substrate at +3.6 V would also require simple buffers to translate the input state voltage to ~-1 V.

Some progress has been made in studying the consequences of defining the duplicating property in terms of the limiting continuous function which is approached by the descrete impulse response ${}_a h_b^2$ in the limit of $a \to \infty$ and the sampling time, τ, being reduced so that $a\tau$ = constant. If it can be successfully implemented, this kind of definition should make it possible to decide the question of the existence of other filter structures with a similar duplicating property, but so far there are several major difficulties to this approach.

In the previous report,[3] the long shift registers should have length k - 1, and the accompanying text should read k = 9.

Filters using decimation of sampling rate have also been considered by Langenthal and Gowrinathan.[4] The time-domain properties such as duplication were not discussed by them, however.

An autocollimator has been built for use in testing the other optical parts of the stellar interferometer. Since one of its purposes is to test the division of power into different parts of the diffraction pattern formed by the beam splitter, a primary goal in the design was to minimize the scattering of light into the image plane by elements between the light source and the element under test, especially the autocollimator's beam splitter.

Figure II-3 is a schematic diagram of the autocollimator. For clarity, it has been drawn cut in half, so that the light path is in or near the plane of the cut.

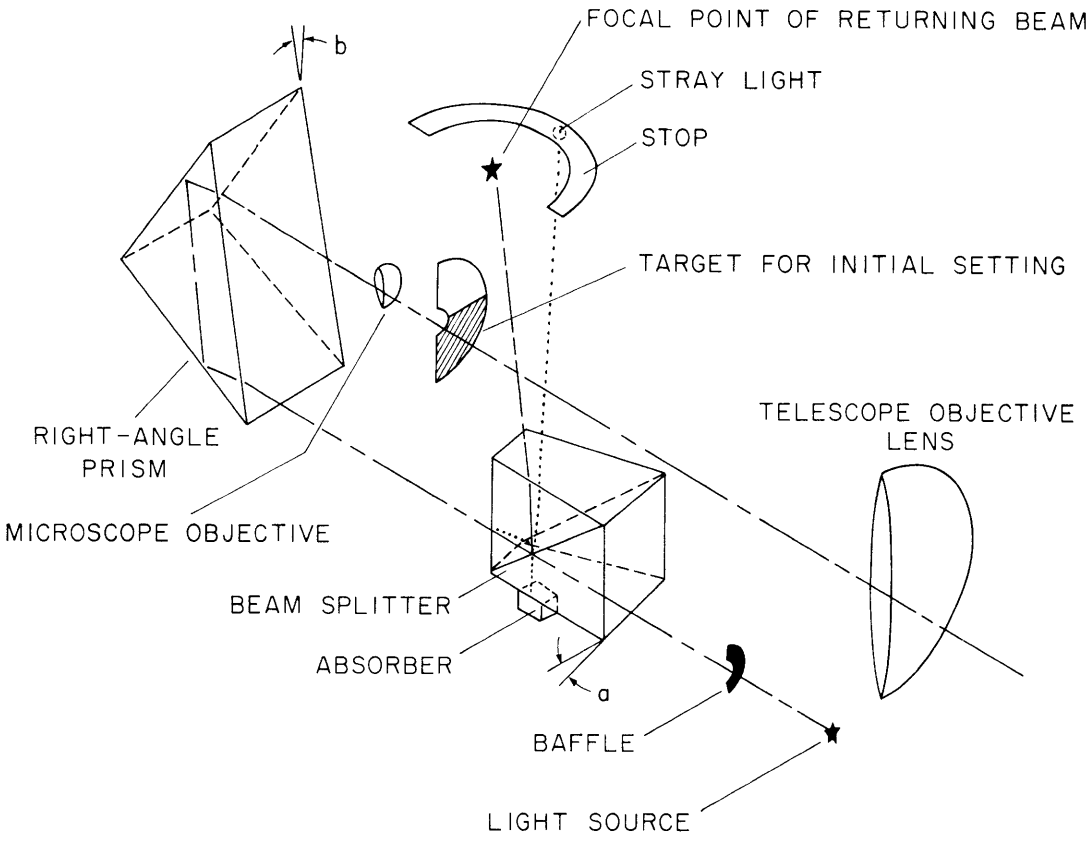

Fig. II-3. The autocollimator.

The beam splitter is a half-silvered prism, with another cemented to it to form a cube. If the light from the source traveled through the cube perpendicular to the faces, then the reflection from the front face of the cube (the face farthest from the light source) would return to the observer and create a very bright background light in the focal plane of the light returning from the element that is being tested. A similar unwanted reflection could occur from the bottom face of the beam splitter, but it is eliminated by the absorber. This background light is prevented by rotating the beam splitter through angle a, 4°15' in this case. This causes the returning beam and the stray light beam to be deflected in opposite directions, and, as drawn, the stray light is absorbed by a stop near the focal plane of the returning light.

Rotating the beam splitter in this way would, by itself, introduce astigmatism into the image that is finally formed, but this is removed by tilting the right-angle prism (the main purpose of which is to fold the light path and reduce the size of the autocollimator) through angle b, 3°. Stray light reflected from the faces of the right-angle

prism is similarly absorbed by the stop. This eliminates astigmatism because a and b are in perpendicular planes, and a ≠ b because the path length in the right-angle prism is longer than in the beam splitter.

The next element is a microscope objective, which is used to increase the effective focal length of the telescope objective. The microscope objective is 40X, n.a. = 0.65, and the telescope objective is 10 in. focal length, f/5. Thus the effective focal length is 400 in.

The oculars used are 10X and 20X, for an overall magnification of 400X and 800X. With such high magnification, it would be difficult initially to locate the image without some auxiliary siting method. This is provided by the target located in the focal plane of the telescope objective. In normal use, the light passes through the hole in the center; for initial alignment, the ocular is removed, and a small lamp shines on the target. In the telescope objective, greatly reduced by the microscope lens, the image of part of the target is seen, reflected in the mirror that is being tested. Once the mirror has been set to the center of the target, the ocular is replaced and the measurement can proceed.

Since the stray light from the beam splitter and right-angle prism has been eliminated, the only remaining source of significant stray light is reflections from the elements in the microscope objective. Although this light is perceptible, it is dim enough to be acceptable for present use.

In the autocollimator only readily available and relatively inexpensive optical parts are used. The mechanical construction is simple and noncritical.

P. L. Kebabian

References

1. P. L. Kebabian, "Stellar Interferometer," Quarterly Progress Report No. 101, Research Laboratory of Electronics, M.I.T., April 15, 1971, pp. 1-11.
2. Ibid., see Fig. I-5, p. 6.
3. Ibid., see Fig. I-10, p. 11.
4. I. Langenthal and S. Gowrinathan, "Advanced Digital Processing Techniques," CFSTI, AD-708-736.
5. M. Habegger, "Astigmatism in Light Deflector Elements," J. Opt. Soc. Am. 60, 326 (1970).

C. INFRARED TRANSMISSION OF CO_2 AND N_2O

In our last report[1] we proposed a method for evaluating the transmission of a Q branch arising from a particular vibration-rotation transition. In reality the transition also gives rise to P and R branches. The complete spectrum contains

strong overlapping P, R, and Q branches arising from different vibration-rotation transitions. For a homogeneous gaseous medium of path length u, the transmittance averaged over the channel $\Delta\omega$ is

$$\tau = \frac{1}{\Delta\omega}\int_{\Delta\omega} d\omega \prod_i \exp\left\{-u\left[k_i^P(\omega)+k_i^R(\omega)+k_i^Q(\omega)\right]\right\}, \tag{1}$$

where

$$k_i^m(\omega) = \sum_J S_{iJ}^m\left[\frac{1}{\pi}\frac{a}{a^2+\left(\omega-\omega_{iJ}^m\right)^2}\right] \qquad m = P, R, Q \tag{2}$$

is the absorption coefficient of one branch. The subscripts iJ refer to a particular line arising from the i^{th} vibration-rotation transition whose lower rotation number is J. The line is centered at frequency ω_{iJ}, has integrated intensity S_{iJ}, and assumes the Lorentz profile of halfwidth a.

We uncouple the different vibration-rotation bands and approximate Eq. 1 by

$$\tau = \prod_i \tau_i^P \tau_i^R \tau_i^Q, \tag{3}$$

where, omitting $d\omega$ in the equations to avoid excessive notation, we have

$$\tau_i^m = \frac{1}{\Delta\omega}\int_{\Delta\omega} \exp\left[-uk_i^m(\omega)\right], \qquad m = P, R, Q. \tag{4}$$

The same approximation is taken in the random Elsasser model. We do not, however, determine τ_i^m by assuming an Elsasser band. Rather, the transmittance τ_i^Q is evaluated as in our last report,[1] and τ_i^P, τ_i^R are computed by the following method.

P and R branches are alike in structure but differ from Q branches in having spectral lines more widely separated. Near the center of a line in the P and R branches, the absorption is due mainly to the line itself and only slightly to the wings of neighboring lines. It is therefore expedient to treat the wing contribution as a correction term. For m = P or R, we have

$$\begin{aligned}\tau_i^m &= \frac{1}{\Delta\omega}\int_{\Delta\omega} \exp\left\{-u\left[\sum_J \frac{S_{iJ}^m}{\pi}\frac{a}{a^2+\left(\omega-\omega_{iJ}^m\right)^2}\right]\right\} \\ &= \frac{1}{\Delta\omega}\sum_J \int_{\Delta\omega_{iJ}} \exp\left\{-u\left[\frac{S_{iJ}^m}{\pi}\frac{a}{a^2+\left(\omega-\omega_{iJ}^m\right)^2}+\sum_{J'\neq J}\frac{S_{iJ'}^m}{\pi}\frac{a}{a^2+\left(\omega-\omega_{iJ'}^m\right)^2}\right]\right\},\end{aligned} \tag{5}$$

where, by choosing J to be the value of J' that minimizes $\left(\omega-\omega_{iJ'}^{m}\right)^2$, we have divided the channel into intervals occupied by different lines. The separation thus far is

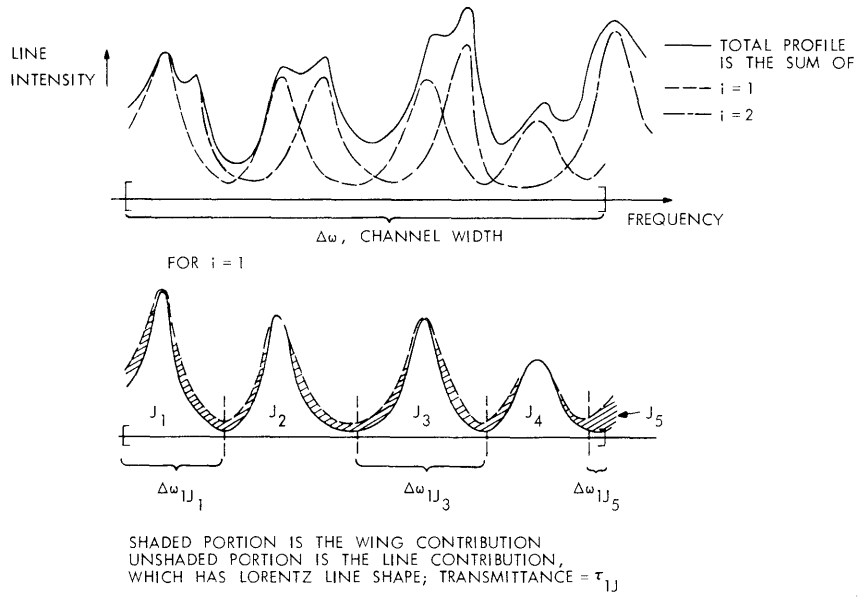

Fig. II-4. Separating two overlapping bands.

illustrated in Fig. II-4 for the case i = 1 and 2, and J running over 5 values when i = 1.

We further approximate Eq. 5 by

$$\tau_i^m = \frac{1}{\Delta\omega} \sum_{J}' e^{-\alpha u \sigma_{iJ}} \int_{\Delta\omega_{iJ}} \exp\left\{-u\left[\frac{S_{iJ}^m}{\pi} \frac{\alpha}{\alpha^2 + \left(\omega-\omega_{iJ}^m\right)^2}\right]\right\}, \tag{6}$$

where

$$\sigma_{iJ} = \sum_{J'\neq J} \frac{S_{iJ'}^m}{\pi} \frac{1}{\left(\omega-\omega_{iJ'}^m\right)^2}$$

represents the wing contribution of lines adjacent to the one centered at ω_{iJ}^m. We have made use of the fact that the separation between lines is much greater than the halfwidth, so that σ_{iJ} can be tabulated for each line in the channel. The integral in Eq. 6 represents the transmittance of a single Lorentz line over a finite spectral interval. Its evaluation was given explicitly in our last report.[2]

This completes the algorithm for computing the transmittance of P and R branches

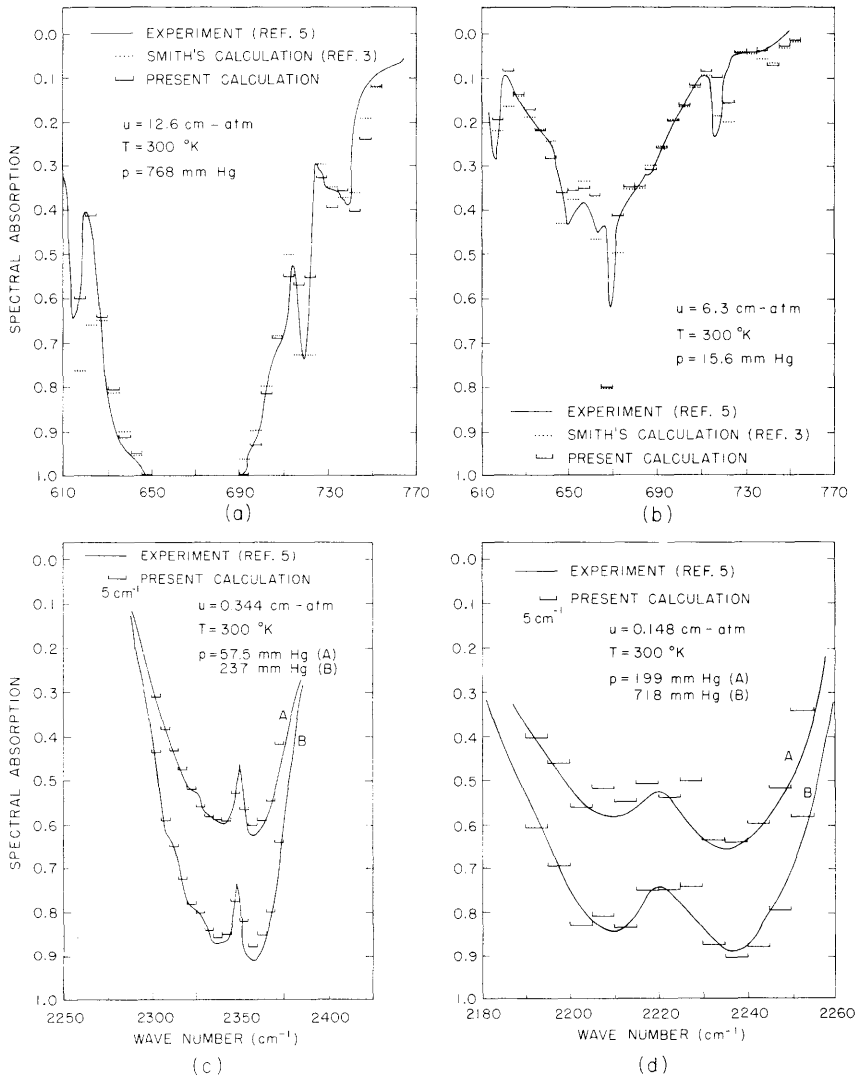

Fig. II-5. (a) Transmission of CO_2 near 15 μ.
(b) Transmission of CO_2 near 15 μ.
(c) Transmission of CO_2 near 4.3 μ.
(d) Transmission of N_2O near 3.9 μ.

over a homogeneous medium. With this procedure, we have evaluated the transmission of CO_2 near 4.3 μ and 15 μ, and N_2O near 3.9 μ. In Fig. II-5 some results are compared with experimental measurements and values calculated by using band models from published work. Agreement is satisfactory over most channels.

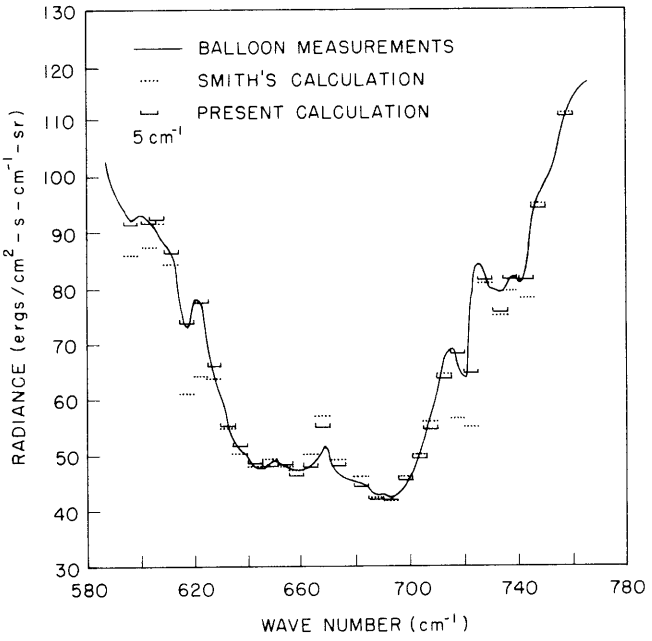

Fig. II-6. Atmospheric radiation: Experimental and calculated.

Up to this point we have considered only homogeneous media. In the atmosphere physical conditions vary. An equivalent set of homogeneous conditions must be defined before the procedure outlined above can be applied to the atmosphere. We have adopted the Curtis-Godson approximation to obtain an equivalent pressure $\bar{p}$ and an equivalent temperature $\bar{T}$:

$$\bar{p} = \int p\, du / \int du$$

$$\bar{T} = \int T\, du / \int du.$$

On May 8, 1966, a NASA balloon-borne interferometer measured several spectra of the upward infrared radiance at the 8 mb pressure level over Palestine, Texas. The main absorbents in this frequency range are carbon dioxide and water vapor. In Fig. II-6, the recorded values are compared with calculation performed under the assumption that the Earth radiates as a blackbody. The dotted lines were obtained by Smith[3] when he compared his polynomial fit with the quasi-random model.[4] We retained

his values for the H_2O transmittance and multiply with it the CO_2 transmittance calculated by using this method. Our results appear to be in better agreement with experiment than those using the polynomial fit for H_2O and CO_2.

R. K. L. Poon, D. H. Staelin

References

1. R. K. L. Poon and D. H. Staelin, "Transmission of Carbon Dioxide: Q Branch," Quarterly Progress Report No. 101, Research Laboratory of Electronics, M.I.T., April 15, 1971, pp. 11-17.
2. Ibid., see Fig. I-11, p. 15.
3. W. Smith, "A Polynomial Representation of Carbon Dioxide and Water Vapor Transmission," National Environmental Satellite Center Technical Report, NESC 47 (1969).
4. P. J. Wyatt, V. R. Stull, and G. N. Plass, "Quasi-random Model of Band Absorption," J. Opt. Soc. Am. 52, 1209 (1962).
5. D. E. Burch, D. A. Gryvnak, and D. Williams, Appl. Opt. 1, 473 and 759 (1962).